

Backscattering enhancement of light by nanoparticles positioned in localized optical intensity peaks

Zhigang Chen, Xu Li, Allen Taflove, and Vadim Backman

We report what we believe to be a novel backscattering phenomenon associated with localized optical intensity peaks (spanning as little as 43 nm) arising at the shadow-side surfaces of plane-wave-illuminated dielectric microcylinders of noncircular cross sections. Namely, for nanometer-scale dielectric particles positioned within the localized intensity peaks, their backscattering of visible light is enhanced by several orders of magnitude relative to the case of isolated nanoparticles (i.e., Rayleigh scattering). The positions of the localized intensity peaks can be quickly scanned along the microcylinder surface by changing either the incident wavelength or angle. This combination of giant backscattering enhancement of nanoparticles and ease and rapidity of scanning may present advantages relative to the use of fragile, mechanically scanned, near-field probes. Potential applications include visible-light detection, characterization, and manipulation of nanoparticles. © 2006 Optical Society of America

OCIS codes: 290.1350, 290.5850, 290.5870, 170.0170.

1. Introduction

In recent years, interest in the spatial distribution of electromagnetic intensity both within and in the near-field regions external to small particles has been growing. This growing interest stems from progress in near-field optics made by the development of both experimental techniques and numerical methods for calculations of near-field structures.¹ It is clear that the curved surface of particles together with the index of refraction discontinuity at the interface alters the spatial distribution of electromagnetic intensity both within the particles and in the near-field regions external to the particles. When the size parameter of the particle (defined as $x = 2\pi a/\lambda$, where a is the characteristic dimension of the particle and λ is the incident wavelength) is much less than unity, i.e., the Rayleigh limit, the internal fields are uniformly distributed and the external near field is only slightly

modulated about the incident-field value by a small scattered field. When the size parameter is much greater than unity, i.e., the geometrical optics limit, a particle can be envisioned as a thick lens. A spot (in the case of spherical lens) or line focus (in the case of cylindrical lens) is located external to such a thick lens, with a size larger than one half wavelength of the incident light.

For spheres and circular cylinders that have intermediate values of the size parameter between the Rayleigh and geometrical optics limits, exact calculations for the spatial distribution of the internal and near-field intensities can be performed using the Mie theory.²⁻⁴ However, for irregularly shaped particles, their scattering properties cannot be obtained analytically, and numerical methods for solving Maxwell's equations are needed in such circumstances.⁵⁻⁷

In this paper, using high-resolution finite-difference time-domain⁸ (FDTD) modeling, we investigate the spatial distributions of the internal and near-external optical intensities of noncircular dielectric microcylinders. We have found that these spatial distributions can be significantly different from those of circular dielectric cylinders.^{2,3,9} One prominent feature is a set of highly localized nanoscale intensity peaks (NIPs) arising along the shadow-side surface of noncircular cylinders. Such NIPs can span as little as 43 nm, and can enhance the backscattering of visible light by nanometer-scale dielectric particles by sev-

Z. Chen (z-chen@northwestern.edu) and A. Taflove are with the Department of Electrical and Computer Engineering, Northwestern University, Evanston, Illinois 60208. X. Li and V. Backman are with the Department of Biomedical Engineering, Northwestern University, Evanston, Illinois 60208.

Received 23 May 2005; revised 3 August 2005; accepted 5 August 2005.

0003-6935/06/040633-06\$15.00/0

© 2006 Optical Society of America

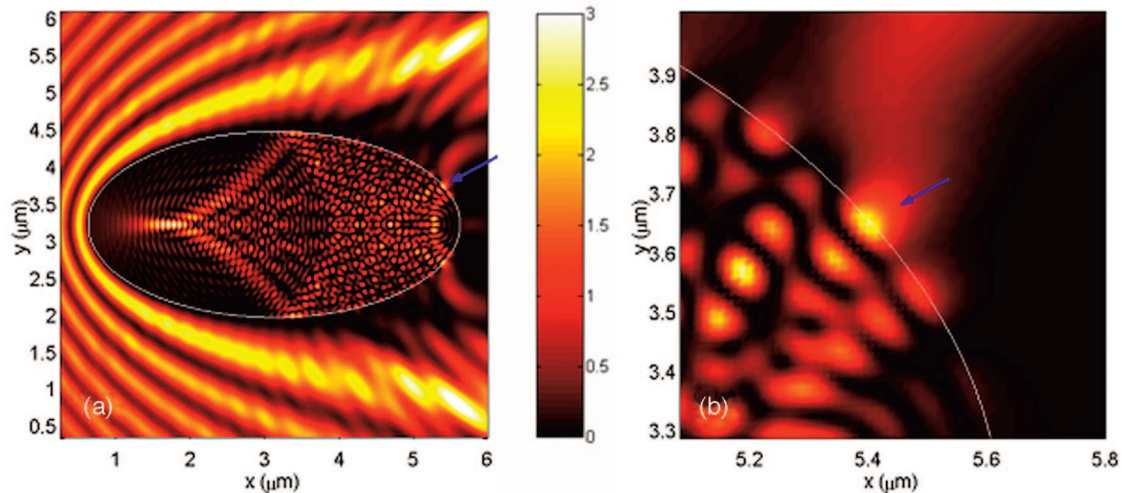


Fig. 1. (Color online) (a) Illustration of optical NIPs, marked by an arrow, at the shadow-side surface of a plane-wave-illuminated elliptical dielectric cylinder. The FDTD-calculated envelope of the sinusoidal steady-state intensity is visualized in linear scale. Light of wavelength $\lambda = 500$ nm propagates from left to right. (b) Expanded view of NIPs at the shadow-side surface of the cylinder in (a).

eral orders of magnitude, which is a fundamental dimensional increase relative to the Rayleigh backscattering. In addition, we have found that the locations of the NIPs can be scanned tangentially along the cylinder surface by changing either the incident wavelength or angle. This combination of giant backscattering enhancement of nanoparticles and ease and rapidity of scanning may present advantages relative to the use of fragile, mechanically scanned, near-field probes. Potential applications of this phenomenon include visible-light detection, characterization, and manipulation of nanoparticles.

2. Localized Nanoscale Intensity Peaks

By using high-resolution FDTD numerical solutions of Maxwell's equations, we first study the internal and near-external field distributions of plane-wave-illuminated dielectric microcylinders of elliptical and triangular cross sections. Previously, the FDTD method has shown promise in calculating scattering by realistic particles because of its ability to model complex surface shapes and internal structures.^{5–7} The two-dimensional (2D) transverse magnetic (TM) case is considered in the present paper, i.e., wherein the incident magnetic field vector is perpendicular to the axis of the cylinder.

Our FDTD computer code has been verified by calculating the differential scattering cross section of several homogeneous circular dielectric cylinders and comparing these results to the exact analytical solution based on the separation-of-variables method. In terms of the scattered intensity I_s , the incident intensity I_i , and the distance r from the scatterer to the detector, the differential scattering cross section σ_d is defined as

$$\sigma_d = r^2 I_s / I_i. \quad (1)$$

Physically, it specifies the angular distribution of the

scattered light: the amount of light (for unit incident intensity) scattered into a unit solid angle about a given direction.

The perfectly matched layer absorbing boundary condition⁹ is used in our FDTD simulations to efficiently terminate the outer boundary of the computational lattice. With the FDTD space lattice having a uniform square cell size of 1.25 nm (finer than 1/100 of a dielectric wavelength for all computer runs), the results for the differential scattering cross section agree with the exact solution to within ± 1.5 dB over the entire range of scattering angles for all cases studied. Typical computational dynamic ranges for this level of agreement are 60 dB.

Having validated the FDTD numerical modeling procedure, we proceed to study in detail the internal and near-external field distribution of a plane-wave-illuminated homogeneous elliptical-cross-section dielectric cylinder. Figure 1 shows key results that illustrate the spatial distribution of the internal and near-field intensity of an elliptical dielectric cylinder. In this case, we consider an infinite dielectric elliptical cylinder having axes of length 5 and 2.5 μm and a refractive index $n = 3.5$ surrounded by a vacuum medium of a refractive index 1.0. The cylinder is normally illuminated by a rightward-propagating sinusoidal plane wave of wavelength $\lambda = 500$ nm.

Figure 1(a) visualizes the FDTD-calculated envelope of the sinusoidal steady-state intensity (defined as the square of the optical electric field) in linear scale, where the incident intensity is normalized to be unity. It is clear that the intensity distribution of the elliptical cylinder is significantly different from that of the corresponding circular cylinder, which can have a localized jetlike intensity pattern.¹⁰ Furthermore, it is evident that a series of strong NIPs exist at the shadow-side surface of the cylinder, one of which is marked with an arrow. Figure 1(b) shows an expanded view of several NIPs. The strongest NIP,

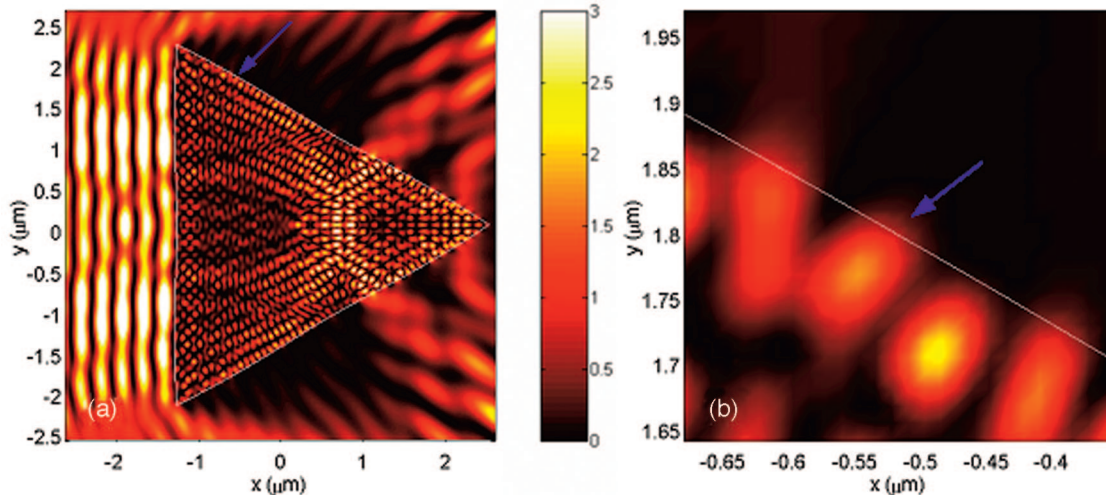


Fig. 2. (Color online) (a) Illustration of optical NIPs, marked by an arrow, at the shadow-side surface of a plane-wave-illuminated triangular dielectric cylinder. The FDTD-calculated envelope of the sinusoidal steady-state intensity is visualized in linear scale. Light of wavelength $\lambda = 500$ nm propagates from left to right. (b) Expanded view of NIPs in (a).

marked with an arrow in Fig. 1, has a full width at half-maximum (FWHM) span of about 80 nm in the tangential direction along the cylinder surface.

The size of the NIPs shown in Fig. 1 can be reduced by adjusting the eccentricity of the elliptical cylinder. Our parametric studies reveal that a NIP spanning only about 56 nm can be obtained using an elliptical cylinder having axes of length 6 and 2.5 μm and refractive index of $n = 3.5$ embedded within an infinite vacuum medium of refractive index 1.0.

According to the uncertainty relation of the Fourier transform, the variation of spatial frequency Δk and the variation of real space Δr satisfy

$$\Delta k \cdot \Delta r \geq \pi, \quad (2)$$

where $\Delta k = 2k = 4\pi/\lambda$. Therefore, Δr has a minimum given by

$$\Delta r \geq \pi/\Delta k = \lambda/4, \quad (3)$$

that is, the minimum size of a beam synthesized by the superposition of optical waves is limited to the order of λ . We note that this is the origin of the diffraction limit. We observe that, considering the wavelength of the incident light in the surrounding medium, the NIPs have sizes of tens of nanometers and are well below the diffraction limit given by Eq. (3). However, if we instead consider the wavelength inside the dielectric microcylinder, the NIP sizes are comparable with the diffraction limit. In this sense, an analogy can be drawn between the NIPs and solid immersion microscopy,¹¹ which takes advantage of the large optical index of a solid immersion lens objective.

Similar to the near-field scanning optical microscopy (NSOM),¹² the subdiffraction-limit feature of the NIPs is due to the presence of evanescent wave components, which can be understood from Eq. (3) in the

case of large variations of the spatial frequency. However, the NIPs distinguish themselves from NSOM in the following sense: The NIPs emerge on smooth dielectric surfaces, whereas NSOM takes advantage of evanescent wave components emerging at sharp metal tips. As a result, the NIPs avoid the manufacturing and operating difficulties inherent in NSOM using fragile nanometer-scale light-emitting tips.

We also repeat similar studies for a plane-wave-illuminated dielectric cylinder having a triangular cross section of side dimension 4.5 μm . Figure 2 shows the internal and near-external intensity distributions of the triangular dielectric cylinder in linear scale. Here the NIP, marked with an arrow, spans only 43 nm in the tangential direction along the cylinder surface.

3. Backscattering Enhancement of Light by Nanoparticles

Now we observe how the backscattering cross section of the dielectric microcylinder is perturbed if a nanoparticle is introduced into the NIP of Fig. 1. The change in the backscattering cross section of the microcylinder caused by the nanoparticle placed at the NIP is defined as the enhanced backscattering cross section of the nanoparticle. We first calculate the differential scattering cross section of the combined system of the microcylinder and nanoparticle where a nanoparticle is placed in the NIP. This differential scattering cross section is denoted as σ_{m+n} . We also calculate the differential scattering cross section of the microcylinder alone, σ_m . The perturbation in the differential scattering cross section of the microcylinder introduced by the nanoparticle is thereof defined as

$$\Delta\sigma = |\sigma_{m+n} - \sigma_m|. \quad (4)$$

Figures 3(a) and 3(b) graph $\Delta\sigma$ within $\pm 10^\circ$ of

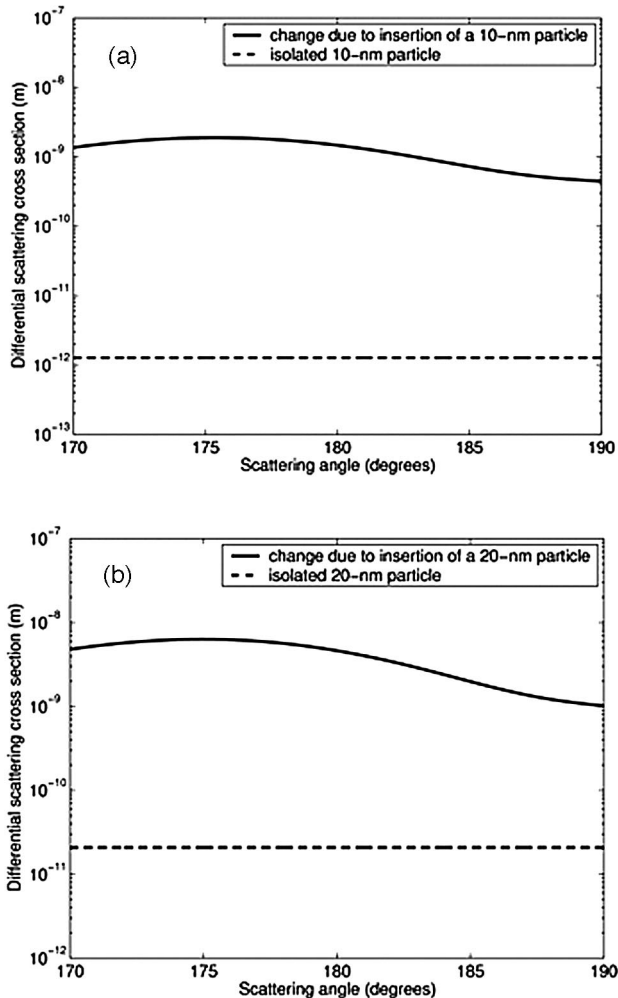


Fig. 3. FDTD numerical results illustrating NIP-enhanced backscattering of light by dielectric nanoparticles. An $n = 1.5$ dielectric nanoparticle of dimension s is located at the center of the NIP at the surface of the cylinder shown in Fig. 1. (a) Absolute value of the change of the differential scattering cross section within $\pm 10^\circ$ of the backscatter of the cylinder for $s = 10$ nm compared with the differential scattering cross section of the isolated nanoparticle. (b) Repeated studies of (a) for a nanoparticle of dimension $s = 20$ nm.

backscatter when a nanoparticle ($n = 1.5$) of dimension $s = 10$ nm and $s = 20$ nm, respectively, are located at the center of the NIP (solid curve). These figures also graph the corresponding differential scattering cross section of the isolated nanoparticle (dashed line). We note that the differential scattering cross section of a nanoparticle is greatly enhanced when it is placed at a NIP. The magnitude of this enhancement depends on the scattering angle and is most significant at an angular cone of about 30° centering the exact backscattering direction. However, the scattering enhancement effect diminishes dramatically at scattering angles beyond this angular cone. Therefore we term it backscattering enhancement based on the fact that the enhancement centers the exact backscattering direction and it is easier to

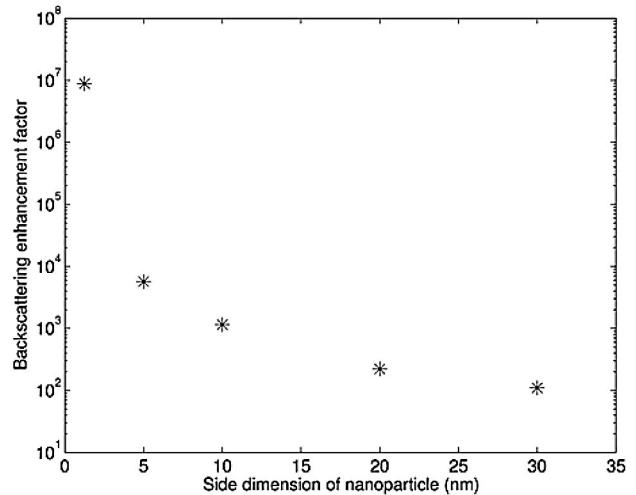


Fig. 4. FDTD numerical results illustrating the backscattering enhancement factor as a function of dimension s of dielectric nanoparticles. An $n = 1.5$ dielectric nanoparticle of dimension s is inserted at the center of the NIP at the surface of the cylinder shown in Fig. 1.

collect the scattered signal at the exact backscattering direction.

From Figs. 3(a) and 3(b) we see that the effective backscattering cross section of each nanoparticle is enhanced by several orders of magnitude due to complex composite mutual interactions of the dielectric microcylinder and the nanoparticle positioned in the NIP. Specifically, the backscattering enhancement is on the order of magnitude of 10^3 for the 10 nm particle and 10^2 for the 20 nm particle. The intensity scales in Figs. 1 and 2 are linear. It is evident that the enhancement of backscattering is much greater than the field enhancement due solely to the microcylinder. Therefore the effective backscattering of the nearby nanoparticle is enhanced by the complex composite mutual interactions between the nanoparticle and microcylinder. The nanoparticle is first excited by the NIP emerging from the microcylinder, and its scattering intensity is elevated by one order of magnitude, as determined by the intensity of the NIP. The fields reradiated by the NIP-excited nanoparticle interact with the normal electromagnetic modes of the microcylinder. This interaction acts to modify the scattering properties of the nanoparticle in such a way as to elevate its backscattered intensity by additional orders of magnitude.

We note that, if the nanoparticle is placed at a minimum in the shadow region, it causes no change in the scattering cross section of the microcylinder. Our further research has shown that, as the nanoparticle is moved away from the center of the NIP, the backscattering enhancement decreases with the decrease of the intensity of the NIP. The nanoparticle alone is effectively invisible. In the case of NSOM, a metal-coated dielectric tip is interposed between the nanoparticle and the observer, allowing the nanoparticle to be sensed. In the present NIPs technique, a dielectric cylinder is similarly interposed between the

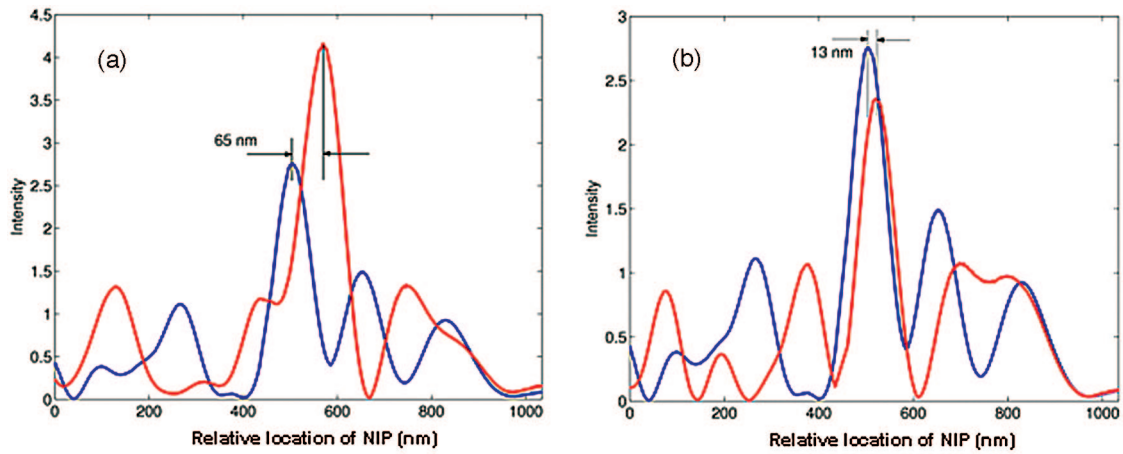


Fig. 5. (Color online) Effects of the perturbing incident wavelength and angle on locations of optical NIPs at the shadow-side surface of a plane-wave-illuminated elliptical cylinder. The FDTD-calculated envelope of the sinusoidal steady-state intensity is visualized. (a) The solid curve corresponds to the incident wavelength of 500 nm whereas the red curve corresponds to the incident wavelength of 525 nm. (b) The solid curve corresponds to the incident angle of 0° , whereas the red curve corresponds to the incident angle of 13° .

nanoparticle and the observer to allow detection. For a 10 nm dielectric particle placed at a NIP, the perturbation of the backscattering cross section of the microcylinder discussed here is about 0.3% of that of the microcylinder without nanoparticle. Such a perturbation is within the dynamic range of available instruments.

From Figs. 3(a) and 3(b) we also see that the dynamic range of the enhanced differential cross section of the 20 nm particle is much wider than that of the 10 nm particle. This could provide a cheap, simple way to sort nanoparticles by their sizes. Further investigation has revealed that this backscattering enhancement also depends on the refractive index of the nanoparticle. Therefore it is viable to sort nanoparticles by their refractive indices by analyzing their NIP-enhanced backscattering cross section.

Figure 4 graphs the backscattering enhancement factor as a function of the size of the nanoparticle. The backscattering enhancement factor (BEF) is defined as

$$\text{BEF} = \Delta\sigma / \sigma_n, \quad (5)$$

where σ_n represents the differential scattering cross section of the isolated nanoparticle. From Fig. 4 we observe that the NIP created by the much larger microcylinder provides a significant dimensional increase in the effective backscattering cross section of the nanoparticle relative to the case where the nanoparticle is isolated (i.e., Rayleigh scattering). The backscattering cross section of light by particles of size between 30 and 1 nm is enhanced by 2–7 orders of magnitude. This backscattering enhancement is a combined effect of the large local fields (i.e., NIPs) and complex composite interactions between the closely spaced microcylinder and nanoparticle.

4. Scanning of the Positions of Nanoscale Intensity Peaks

We further investigate how the positions of the NIPs change along the microcylinder surface if one adjusts the incident wavelength or angle. Here we consider the NIP in Fig. 1. Figure 5(a) illustrates the effect of perturbing the incident wavelength on the location of a NIP along the cylinder surface in Fig. 1. Here the

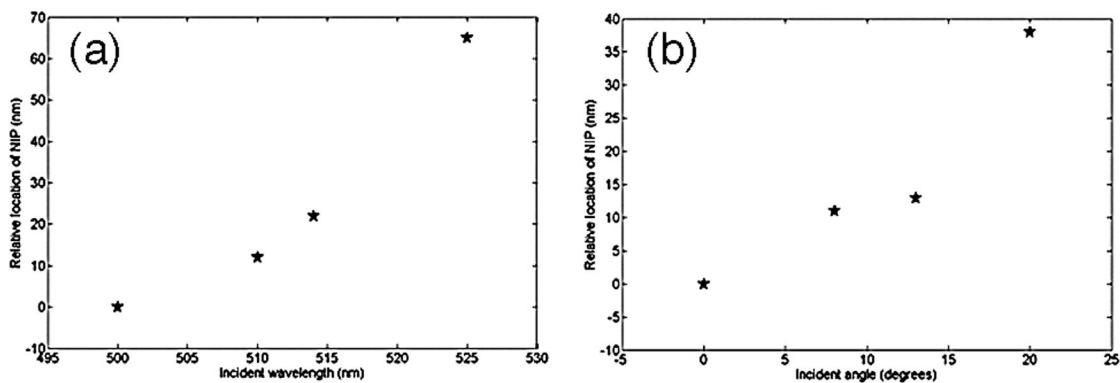


Fig. 6. Effects of the perturbing incident wavelength and angle on locations of optical NIPs at the shadow-side surface of a plane-wave-illuminated elliptical cylinder. The relative location shift of a NIP is plotted. (a) Effects of perturbing incident wavelength on locations of NIPs. (b) Effects of perturbing incident angle on locations of NIPs.

solid curve corresponds to an incident wavelength of 500 nm whereas the dotted curve corresponds to an incident wavelength of 525 nm. From Fig. 5(a) we see that the tangential location of the NIP is shifted by 65 nm for an incident wavelength perturbation of 25 nm.

Figure 5(b) illustrates the effect of perturbing the incident angle on the location of a NIP along the cylinder surface in Fig. 1. Here the solid curve corresponds to the incident angle of 0° whereas the dotted curve corresponds to the incident angle of 13° . From Fig. 5(b) we see that the tangential location of the NIP is shifted by 13 nm for an incident angle perturbation of 13° .

Figure 6 shows the relative location of a NIP as a function of incident wavelength from 500 to 525 nm [Fig. 6(a)] and as a function of incident angle from 0° to 20° [Fig. 6(b)]. Here we observe a monotonic variation of the NIP location with respect to the wavelength and incident-angle perturbations. This can provide a simple and efficient way to scan the NIP across the position of a fixed nanoscale structure located at the cylinder surface, thereby rendering an image of the nanostructure. In principle, such scanning could be accomplished purely optically (i.e., with no mechanical movement) by using either a variable-wavelength light source or a white light source in combination with a wavelength-selective detector. It should be noted that this kind of scanning is different from that in the NSOM.

5. Conclusion

We have investigated the spatial distributions of the near-field and internal electromagnetic intensities of noncircular dielectric microcylinders that have intermediate values of size parameter between the Rayleigh and geometrical optics limits. We have found that the spatial distributions of the near-field and internal electromagnetic intensities of noncircular dielectric cylinders are significantly different from those of their circular counterparts. One prominent feature of the calculated intensity distribution of noncircular dielectric cylinders is the highly localized NIPs generated at the shadow-side surfaces. The sizes of the NIPs are well below the diffraction limit of light.

We have further observed that such NIPs can enhance the backscattering of visible light by nanometer-scale dielectric particles located within the NIPs by several orders of magnitude. The order of magnitude of the enhancement depends on the size and refractive index of nanoparticles. This backscattering enhancement is a combined effect of the large local fields (i.e., NIPs) and complex composite inter-

actions between the closely spaced microcylinder and nanoparticle. In addition, the positions of the localized intensity peaks can be quickly scanned along the microcylinder surface by changing either the incident wavelength or angle. This combination of giant backscattering enhancement and ease and rapidity of scanning may present advantages relative to the use of fragile, mechanically scanned, near-field probes. We believe that the backscattering enhancement phenomenon discussed in this paper provides potential applications in visible-light ultramicroscopy wherein nanoparticles consisting of as few as several hundred atoms could be detected and characterized. Other potential applications include manipulation and modification of similarly sized nanoparticles.

This work was supported by National Science Foundation grant BES-0238903.

References

1. M. A. Paesler and P. J. Moyer, *Near-Field Optics: Theory, Instrumentation, and Applications* (Wiley, 1996).
2. J. F. Owen, R. K. Chang, and P. W. Barber, "Internal electric field distributions of a dielectric cylinder at resonance wavelengths," *Opt. Lett.* **6**, 540–542 (1981).
3. D. S. Benincasa, P. W. Barber, J.-Z. Zhang, W.-F. Hsieh, and R. K. Chang, "Spatial distribution of the internal and near-field intensities of large cylindrical and spherical scatters," *Appl. Opt.* **26**, 1348–1356 (1987).
4. X. Li, Z. Chen, A. Taflove, and V. Backman, "Optical analysis of nanoparticles via enhanced backscattering facilitated by 3D photonic nanojets," *Opt. Express* **13**, 526–533 (2005).
5. Z. Chen, A. Taflove, and V. Backman, "Concept of the equiphase sphere for light scattering by nonspherical dielectric particles," *J. Opt. Soc. Am. A* **21**, 88–97 (2004).
6. X. Li, Z. Chen, A. Taflove, and V. Backman, "Novel analytical techniques to address forward and inverse problems of light scattering by irregularly shaped particles," *Opt. Lett.* **29**, 1239–1241 (2004).
7. X. Li, Z. Chen, A. Taflove, and V. Backman, "Equiphase-sphere approximation for analysis of light scattering by arbitrarily-shaped nonspherical particles," *Appl. Opt.* **43**, 4497–4505 (2004).
8. A. Taflove and S. Hagness, *Computational Electrodynamics: The Finite-Difference Time-Domain Method* (Artech House, 2000).
9. Z. Chen, A. Taflove, and V. Backman, "Photonic nanojet enhancement of backscattering of light by nanoparticles: a potential novel visible-light ultramicroscopy technique," *Opt. Express* **12**, 1214–1220 (2004).
10. J.-P. Berenger, "A perfectly matched layer for the absorption of electromagnetic waves," *J. Comput. Phys.* **114**, 185–200 (1994).
11. S. M. Mansfield and G. S. Kino, "Solid immersion microscope," *Appl. Phys. Lett.* **57**, 2615–2616 (1990).
12. B. Dunn, "Near-field scanning optical microscopy," *Chem. Rev.* **99**, 2891–2928 (1999).